PHYSICAL REVIEW A VOLUME 57, NUMBER 1 JANUARY 1998

Comparative study of Si-$2p$ core-excitation spectra in the tetrahedral molecules SiX_4 (with X=H, D, F, Cl, Br, CH_3)

Ralph Püttner, Michael Domke, and Günter Kaindl
Institute of Experimental Physics and Material Science Center, Freie Universität Berlin, Arnimallee 14,
D-14195 Berlin-Dahlem, Germany

(Received 21 August 1997)

High-resolution Si-$2p$ photoabsorption spectra of SiX_4 molecules (X=H, D, F, Cl, Br, CH_3) are presented. High-resolution spectra were obtained for $SiBr_4$ and $Si(CH_3)_4$, and they are compared to the Si-$2p$ spectra of the other SiX_4 molecules studied before. In all cases, vibrational fine structure of the Rydberg states could be resolved, allowing a derivation of vibrational energies and intramolecular distances of the core-excited molecules from Franck-Condon analyses. The results obtained for the various ligand atoms are compared with each other, and are discussed in the context of the equivalent-cores approximation. A detailed analysis of the core-to-valence excitations in all SiX_4 molecules studied is also given.
[S1050-2947(98)06001-6]

PACS number(s): 33.80.Eh, 33.20.Rm, 33.20.Tp, 33.15.Dj

I. INTRODUCTION

Core-excitation spectra of silicon-containing molecules have been investigated by photoabsorption and photoemission for quite a few molecules in the past. For deep core excitations (Si $1s$, $h\nu \cong 1850$ eV), the spectra were found to depend only slightly on the ligand atom [1], while, for Si-$2p$ excitations at $h\nu = 100-110$ eV, strong changes with the ligand atom were found [1–14]. In recent years, substantial progress has been achieved in high-resolution photoabsorption spectroscopy, which even allowed us to separate vibrational substates of core excited Rydberg states. Even in earlier photoemission [13,14] and photoabsorption [2–5] spectra with moderate resolution, vibrational substates could be resolved in cases of low-mass ligands (X=H, D, partly F) with relatively large vibrational energies. Vibrations of heavy ligands, however, can be discerned only with high resolution: well-separated vibrational substates have been resolved recently by photoabsorption for SiF_4 [15], for $SiCl_4$ [16], and also in a preliminary way for $SiBr_4$ [17].

In the present paper, this systematic study of vibrationally resolved spectra is extended to $SiBr_4$ and $Si(CH_3)_4$. The spectra are subjected to Franck-Condon analyses, resulting in geometrical information for the excited state. The derived vibrational energies and equilibrium distances in the core-excited states of SiH_4, SiD_4, $Si(CH_3)_4$, SiF_4, $SiCl_4$, and $SiBr_4$ are discussed in a comparative way, also in connection with vibrationally unresolved photoabsorption spectra of $Si(CH_3)_4$ [7,9], SiF_4 [4–7,13], and $SiCl_4$ [8–10], as well as photoemission spectra of $Si(CH_3)_4$ [14], SiF_4 [13,14], and $SiCl_4$ [14].

II. EXPERIMENT AND DATA FITTING PROCEDURE

The measurements were performed with the high-resolution plane-grating SX700/II monochromator operated by the Freie Universität Berlin at the Berliner Elektronenspeicherring für Synchrotronstrahlung. A 2442 lines/mm grating was employed, resulting in a resolution of $\leqslant 15$ meV (fullwidth at half maximum) at $h\nu \cong 110$ eV [18]. Photoabsorption was recorded as a function of photon energy by measuring the photoion current using a 10-cm-long gas-ionization cell separated from the ultrahigh vacuum of the monochromator by a 1200-Å thick carbon window. The photon energy was calibrated by monitoring the N $1s^{-1}\pi^*(v''=0 \rightarrow v'=0)$ state of N_2 at $h\nu = 400.88$ eV [19]. The silicon compounds were studied in the gas phase, with typical pressures of $\cong 0.1$ mbar, which assures negligible saturation effects. The chemical stability of the studied compounds was demonstrated by the absence of changes with time of the photoionization spectra.

The observed spectral lines have Voigt profiles, which originate from the convolution of a Lorentzian profile due to the lifetime width Γ, with an approximate Gaussian profile due to monochromator resolution ΔE. The high monochromator resolution of the present study allows us to separate the vibrational substates for all given molecules. The vibrationally resolved spectra were subjected to Franck-Condon analyses, following the algorithm first given by Hutchisson [20,21]. In this procedure, essentially the overlap of the initial ground-state vibrational wave function with the final excited-state vibrational wave functions is fitted to the envelopes of the vibrational bands. Generally, only vibrational sidebands are expected, when sufficiently large differences in the normal coordinate, e.g., the equilibrium distances, between ground state and excited state occur. The relative intensities of the vibrational substates in the excited state, $v' = 0,1,2,...$, depend on the Franck-Condon parameters in the excited state, the vibrational energy $\hbar\omega'$, the anharmonicity $x\hbar\omega'$, and the equilibrium distance R_e. For the calculations, literature values for the ground-state vibrational energies, $\hbar\omega''$, as well as the equilibrium distances, R_g, were used. In the case of well-separated $v' \geqslant 2$ substates, a value for the anharmonicity and hence the sign of the change of the equilibrium distance can be derived. The ground-state anharmonicity $(x\hbar\omega)''$ is usually set to zero, since only $v''=0$ and low v'' values are occupied. For all molecules, hot bands

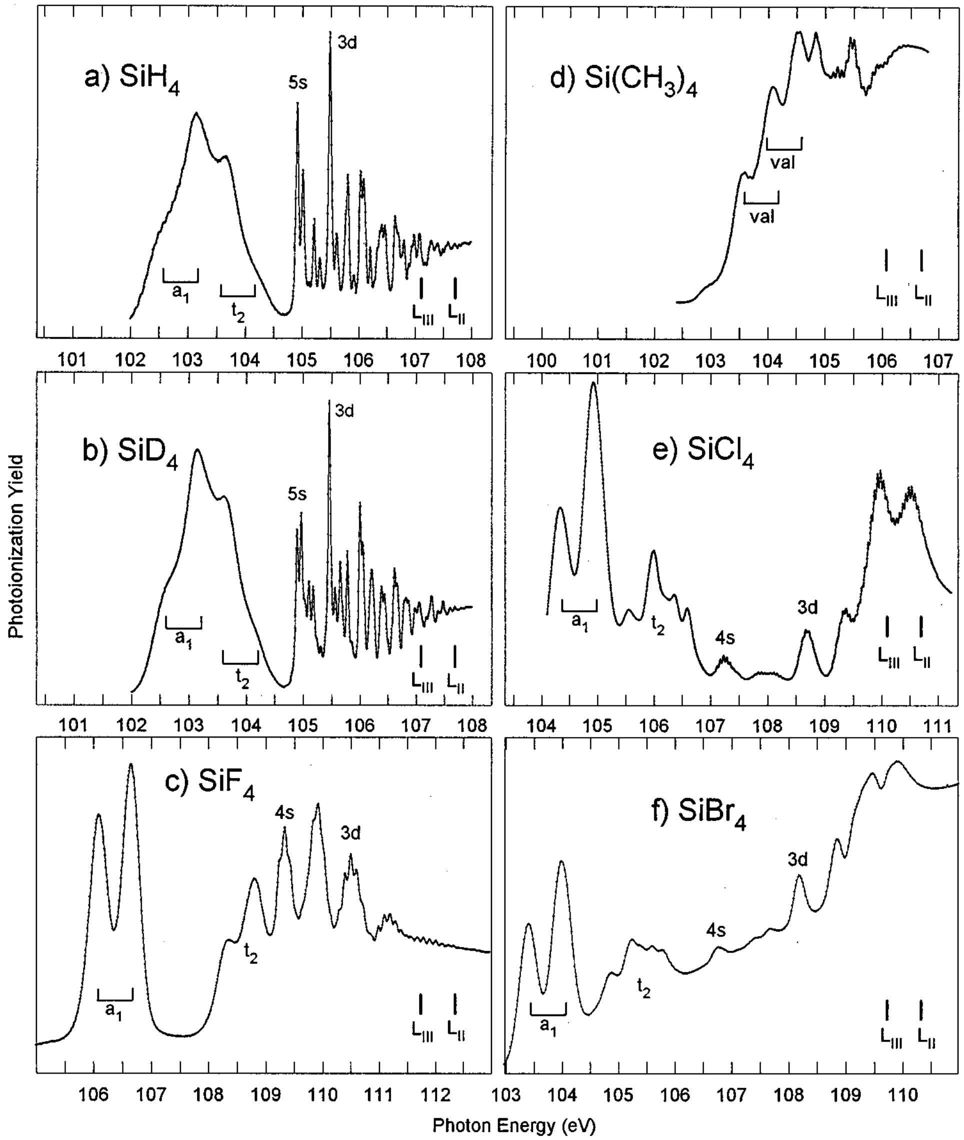

FIG. 1. Overview of the Si-2p core-excitation spectra of tetrahedral silicon molecules, in appropriate 8-eV energy windows. The spectra are ordered in the sequence of decreasing vibrational energies of the symmetric-stretching vibrational mode, i.e., in the sequence SiH_4, SiD_4, SiF_4, $Si(CH_3)_4$, $SiCl_4$, and $SiBr_4$. In the low-energy region, valence transitions (Si $2p^{-1}$ val) are marked; in the Rydberg region, typical $2p_{3/2}^{-1}ns$, nd excitations are marked by ns, nd.

were included in the Franck-Condon analysis, i.e., excitations from a vibrationally excited ground state, $v''=1,2\rightarrow v'=0,1,2,3,\ldots$. Such hot bands are not important for large vibrational splittings $\hbar\omega''$ in the ground state.

III. Si-2p PHOTOABSORPTION SPECTRA

In Fig. 1, an overview of the Si-2p excitation spectra of SiH_4, SiD_4, SiF_4, $Si(CH_3)_4$, $SiCl_4$, and $SiBr_4$ are shown over 8-eV energy regions. These 8-eV energy windows are at slightly different energies for the various molecules due to different chemical shifts caused by the ligands. The Si-2p spectral features exhibit a spin-orbit splitting of $\cong$600 meV between the $2p_{3/2}^{-1}$ and $2p_{1/2}^{-1}$ states, converging towards the L_{III} and L_{II} thresholds, respectively. In the low-energy spectral region, typical spin-orbit splittings are marked by connected vertical-bar diagrams. The spectra are separated in broad $2p\rightarrow$valence excitations ($2p^{-1}$ val, with a_1 and t_2 symmetries, which are in most cases dissociative) and in narrow and long-lived $2p\rightarrow$Rydberg transitions ($2p^{-1}$ Ryd), where typical $2p_{3/2}^{-1}ns$, nd transitions are marked. The Si-2p^{-1} val excitations occur in the low-energy region, below 5 s in silane and 4 s in SiF_4, $SiCl_4$, and $SiBr_4$.

In addition, shape resonance features around the ionization thresholds are visible in the spectra of molecules with large equilibrium distances of $R_g\cong 2$ Å at 106.0, 110.5, and 110.0 eV for $Si(CH_3)_4$, $SiCl_4$, and $SiBr_4$, respectively; these shape resonances overlap with vibrationally split Rydberg states. The energy of a shape resonances correlates with the internuclear distance [22], since shape resonances have their origin in excited electrons trapped by a centrifugal barrier in a region of space with molecular dimensions [23]. As a consequence, the shape resonance of SiF_4 is shifted to higher energies ($h\nu \cong 120$ eV [6]; not shown in the present work), due to a smaller $R_g \cong 1.5$ Å. For light ligand atoms, like in silane, no shape resonances are observed. Note that in most cases the spin-orbit-split $2p^{-1}a_1$ valence excitation is the most intense spectral feature, but its assignment is uncertain in the cases of SiH_4, SiD_4, and $Si(CH_3)_4$. The a_1 valence states in silane (SiH_4,SiD_4) were assigned in agreement with Ref. [24], but they cannot be assigned unambiguously in case of $Si(CH_3)_4$. Obviously, the energy distance of a_1 and t_2 is small for SiH_4 and SiD_4 and large for SiF_4, $SiCl_4$, and $SiBr_4$; this gives a decrease in the $a_1 - t_2$ difference for decreasing electronegativity of the ligands [25], which is reflected by decreasing threshold energies (see Fig. 1). As a consequence, in $Si(CH_3)_4$ the a_1 and t_2 differences might lead to a reversal of the orbital order.

For the Rydberg states, the vibrational substates could be resolved. Except for these substates, the spectra are very similar to previous medium-resolution results for SiH_4, SiD_4 [2–4], SiF_4 [6], $Si(CH_3)_4$ [9], and $SiCl_4$ [9], where in most cases vibrational features were not resolved. We would like to point out some typical observations in the present spectra: For SiH_4 and SiD_4, the lowest Rydberg transition $2p_{3/2}^{-1}5s$ shows different vibrational splittings in the energy region between 104.9 and 105.4 eV. In the cases of SiF_4 and $Si(CH_3)_4$, the vibrational fine structure *gradually* develops, it is first visible for the $4s/3d$ excitations of SiF_4 at $h\nu = 109.2$–110.8 eV and are also resolved for the $3d(e)/4d(e)$ excitations of $Si(CH_3)_4$ at $h\nu = 104.3$–105.0 eV. For $SiCl_4$, the vibrational fine structure appears *suddenly* in the $4s$ excitations at $h\nu = 107.0$ eV. For $SiBr_4$, the vibrational substates are masked due to their small energy differences; however, they will be clearly visible in an expanded spectrum discussed further below.

A. Tetramethylsilane, $Si(CH_3)_4$

Tetramethylsilane (TMS) is a very stable molecule, despite its multiatomic nature; it is used as a calibrant in NMR spectroscopy, and it is also stable on Si-$2p$ core excitation. In Fig. 2, the Si-$2p$ core-excitation spectrum of $Si(CH_3)_4$ is shown in more detail, together with the results of our analysis. A rather complicated sequence of valence and Rydberg orbitals is observed: The most prominent Rydberg states are spin-orbit-split nd states converging towards the L_{III} and L_{II} thresholds. These Si-$2p^{-1}nd$ states are additionally symmetry split into $nd(e)$ and $nd(t_2)$ states, characterized by quantum defects of $\delta(e) = 0.2$ and $\delta(t_2) = -0.3$. The broad spectral feature at $h\nu = 102.8$ eV is assigned to the $2p_{3/2}^{-1}4s$ Rydberg state on the basis of its quantum defect $\delta = 1.96$; this Rydberg state has been moved to an energy far below the region of valence states, which start at $h\nu \geqslant 103.5$ eV. The results of the fit analysis for the nd Rydberg states are given in Table I. From this assignment, and using the Rydberg formula $E = I - R/(n-\delta)^2$ (with $R = 13.605$ eV, and where I is the ionization threshold), we obtained the L_{III} and L_{II} ionization thresholds $I_p(\frac{3}{2}) = 106.075 \pm 0.030$ meV and $I_p(\frac{1}{2}) = 106.700 \pm 0.030$ meV.

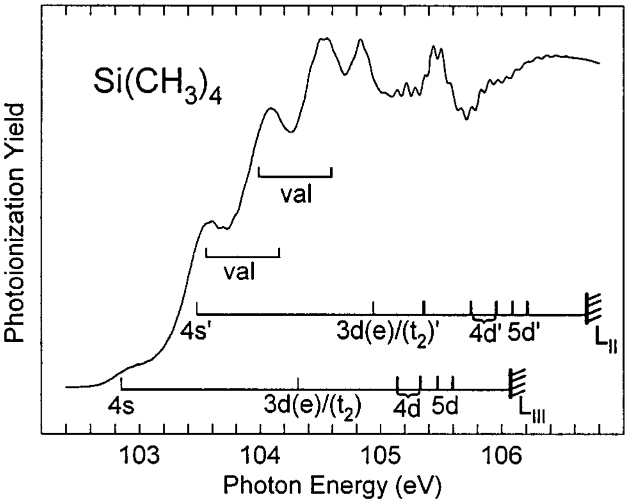

FIG. 2. Photoionization spectrum of Si-$2p$ core-excitation in $Si(CH_3)_4$. The valence states "val" of a_1 and t_2 symmetries as well as the Rydberg states $4s$, $nd(e)$, and $nd(t_2)$, are represented by the vertical-bar diagrams. For the Rydberg states, the vertical bars mark the $v'' = 0 \rightarrow v' = 0$ excitation, with the bold bars representing fit results and the light bars marking estimated values.

In Fig. 3, the Rydberg region of the Si-$2p$ excitations of $Si(CH_3)_4$ is shown in greater detail. The spectral features, with an appropriate number of Rydberg states and their vibrational sidebands, were fitted by a Franck-Condon procedure. It is obvious that only a single vibrational mode is excited in each case, i.e., *only* one normal coordinate is changed upon excitation. TMS has 19 normal vibrational modes; three of them have a_1 symmmetry and are symmetry allowed due to the selection rules of the given molecular symmetry. On the basis of the measured vibrational energy ($\hbar\omega' \cong 75$ meV), we assume excitations of the ω_3 normal mode with a ground-state energy of $\hbar\omega'' = 73.47$ meV [26]: The normal coordinate Q_3 is changed according to $\Delta Q_3 = Q_3' - Q_3'' \neq 0$. For all other normal coordinates Q_j, ΔQ_j is close to zero, below our limit of detection.

To understand the geometrical changes represented by a change of the normal coordinate Q_3, we can restrict our considerations to the three symmetry and normal coordinates with a_1 symmetry and define a symmetry-coordinate vector $\mathbf{S}_i = (S_1, S_2, S_3)$ and a normal-coordinate vector $\mathbf{Q}_j = (Q_1, Q_2, Q_3)$. The three elements of the symmetry-coordinate vector are S_1 describing equal changes in the C-H distances, S_2 describing equal changes in the Si-C-H angles as well as the H-C-H angles by equal amounts, but opposite

TABLE I. Excitation energies (in eV) between the vibrational ground states ($v'' = 0 \rightarrow v' = 0$) of the $2p_{3/2}^{-1}nd$ and $2p_{1/2}^{-1}nd$ Rydberg states, quantum defects δ, and ionization thresholds I_p of $Si(CH_3)_4$, as obtained from the least-squares fit analysis. The error bars for the energies are estimated to be ± 10 meV.

	$2p_{3/2}^{-1}$	δ	$2p_{1/2}^{-1}$	δ
$3d(t_2)$			105.365	−0.19
$4d(e)$	105.144	0.17	105.752	0.21
$4d(t_2)$	105.335	−0.29	105.961	−0.29
$5d(e)$	105.476	0.23	106.094	0.26
$5d(t_2)$	105.602	−0.36	106.217	−0.31
I_p	106.075(30)		106.700(30)	

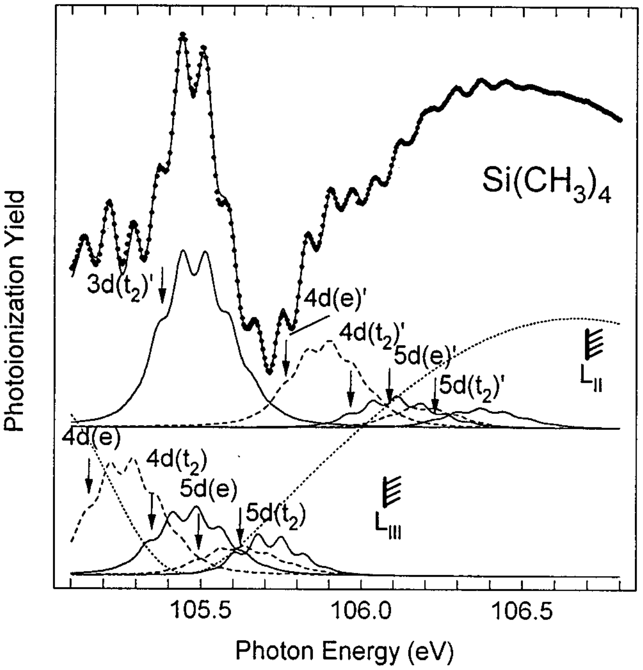

FIG. 3. Rydberg-state section of the Si-$2p$ core-excitation spectrum of Si(CH$_3$)$_4$, and the result of a Franck-Condon analysis represented by the solid line through data points. The solid [dashed] subspectra represent $2p^{-1}nd(t_2)$ [$2p^{-1}nd(e)$] Rydberg states. The observed resonances $2p_{3/2}^{-1}nl$ ($2p_{1/2}^{-1}nl$) are marked by nl (nl'). The dotted curve represents the background regarding Rydberg states in the low-energy region, which have not been fitted, as well as continuum features in the high-energy region. The amplitudes of all subspectra were scaled by a factor $\frac{1}{3}$ with respect to the measured spectrum.

signs, and S_3 describing equal changes of the Si-C distances [27]. The L matrix describes the relation between $\mathbf{S}_i$ and $\mathbf{Q}_j$ by $\mathbf{S}_i = \mathbf{L}_{ij}\mathbf{Q}_j$. For the electronic ground state, the matrix $\mathbf{L}_{ij}$ for the three a_1 coordinates is taken from the literature [27]:

$$L_{ij} = \begin{pmatrix} 1 & 0 & 0 \\ 0 & 1.09 & -0.09 \\ 0 & 0.14 & 0.25 \end{pmatrix}. \tag{1}$$

By assuming equal $\mathbf{L}_{ij}$ for the excited state, we obtain

$$\Delta\mathbf{S}_i = \mathbf{L}_{ij}\Delta\mathbf{Q}_j. \tag{2}$$

The observed ω_3 and the related $\Delta Q_3 \neq 0$ (with $\Delta Q_1 = \Delta Q_2 = 0$) change the Si-C bond distances (S_3 with $L_{33} = 0.25$), the Si-C-H and the H-C-H bond angles (S_2 with $L_{23} = -0.09$), whereas the C-H bond distances remain unchanged (S_1 with $L_{13} = 0$).

The Franck-Condon analysis, taking ground-state values of $\hbar\omega_3'' = 73.47$ meV and R_g(Si-C) = 1.888 Å [26], results in a vibrational energy of $\hbar\omega_3' = 76 \pm 2$ meV for the core-excited state, an anharmonicity of $(x_3\hbar\omega_3)' = 0.3 \pm 0.1$ meV, a decrease of the Si-C bond distance by ΔR(Si-C) = -0.065 Å, a decrease of the Si-C-H angles by 0.5°, and an increase of the H-C-H angles by 0.5°. From the obtained anharmonicity, we determine the sign of the geometrical changes, and by using the formula $D_e = (\hbar\omega)^2/4x\hbar\omega$, we can also derive a value for the dissociation energy, $D_e = 4.8$ eV. The latter can be compared with the results obtained for SiF$_4$ ($D_e = 6.3$ eV) [15] and SiCl$_4$ ($D_e = 5.8$ eV) [16]. The quoted error bars for the fit parameters represent the variety of Franck-Condon results for the different Rydberg states. Note that a suitable Franck-Condon analysis can also be obtained by shifting all $v'' = 0 \rightarrow v' = 0$ excitations by one vibrational quantum to lower excitation energies: This leads to a fit result of only slightly worse χ^2; however, the fitted parameters ΔR(Si-C) $\cong -0.080$ Å and $(x_3\hbar\omega_3)' \cong 0.7$ meV (which is equal to a dissociation energy of $D_e \cong 2$ eV) are unreasonably large as compared to the results for all the other SiX_4 molecules studied so far; consequently, this fit has to be rejected.

B. Silicon (IV) bromide, SiBr$_4$

In the overview spectrum of SiBr$_4$ given in Fig. 1, the valence features Si $2p^{-1}a_1$ and $2p^{-1}t_2$ consist of one spin-orbit-split a_1 feature and a larger number of t_2 structures that will be discussed in Sec. IV. The Si-$2p^{-1}$ Ryd excitations are presented in more detail in Figs. 4 and 5, revealing well-separated vibrational substates with a vibrational energy of ≅33 meV. In Fig. 4, these substates are visible in the energy region from 106.6–107.8 eV, and they are assigned to $2p_{3/2}^{-1}4s$, $2p_{1/2}^{-1}4s$, and $2p_{3/2}^{-1}4p$ excitations. In Fig. 5, vibrational splittings of the $2p_{3/2}^{-1}nd$ and $2p_{1/2}^{-1}nd$ excitations (at $h\nu \geqslant 108.0$ eV) are clearly observed, even though the vibrational substates of the different Rydberg states are only weakly developed, due to a natural lifetime width of ≅40 meV; in addition, the vibrational states overlap strongly. It is impossible to determine the $v'' = 0 \rightarrow v' = 0$ excitations unambiguously from the spectra in Figs. 5(a) and 5(b); therefore, we can only approximately assign the various Rydberg states in the spectra. This ambiguity renders it impossible to calculate the ionization thresholds on the basis of the Rydberg formula; we hence use the following arguments to obtain estimates of the ionization thresholds: The three fitted Rydberg states $2p_{3/2}^{-1}4s$, $2p_{1/2}^{-1}4s$, and $2p_{3/2}^{-1}4p$ are all at excitation energies, which are smaller by 375 meV than in SiCl$_4$; we also transfer this energy shift between SiCl$_4$ and SiBr$_4$ to the $2p_{3/2}^{-1}nd$ and $2p_{1/2}^{-1}nd$ series. This then leads to estimated $v'' = 0 \rightarrow v' = 0$ excitation energies of the $2p^{-1}nd$ states, which are a few tens of meV too high: This can be seen, e.g., with the $2p_{3/2}^{-1}4d$ state, with the $v'' = 0 \rightarrow v' = 0$ excitation at ≅108.90 eV, while distinct vibrational fine structures of this state are observed at $h\nu \cong 108.85$ eV. As a consequence, we assume the L_{III} and L_{II} ionization threshold energies to be 425±50 meV below the SiCl$_4$ values: for SiBr$_4$, we then obtain $I_p(\frac{3}{2}) = 109.675 \pm 0.050$ meV and $I_p(\frac{1}{2}) = 110.275 \pm 0.050$ meV.

We find that, in all Rydberg states, a single vibrational mode is excited, with a vibrational energy close to that of the normal mode a_1 in the ground state of SiBr$_4$, with $\hbar\omega_1'' = 30.87$ meV [28]. The solid curves and the subspectra in Fig. 4 are the results of a Franck-Condon analysis, taking this $\hbar\omega_1''$ value and a ground-state equilibrium distance of $R_g = 2.150$ Å [29]. The Franck-Condon fits were restricted to $2p_{3/2}^{-1}4s$, $2p_{3/2}^{-1}4p$, and $2p_{1/2}^{-1}4s$ states, resulting in vibrational energies of $\hbar\omega_1' = 33.6 \pm 0.5$ meV and equilibrium

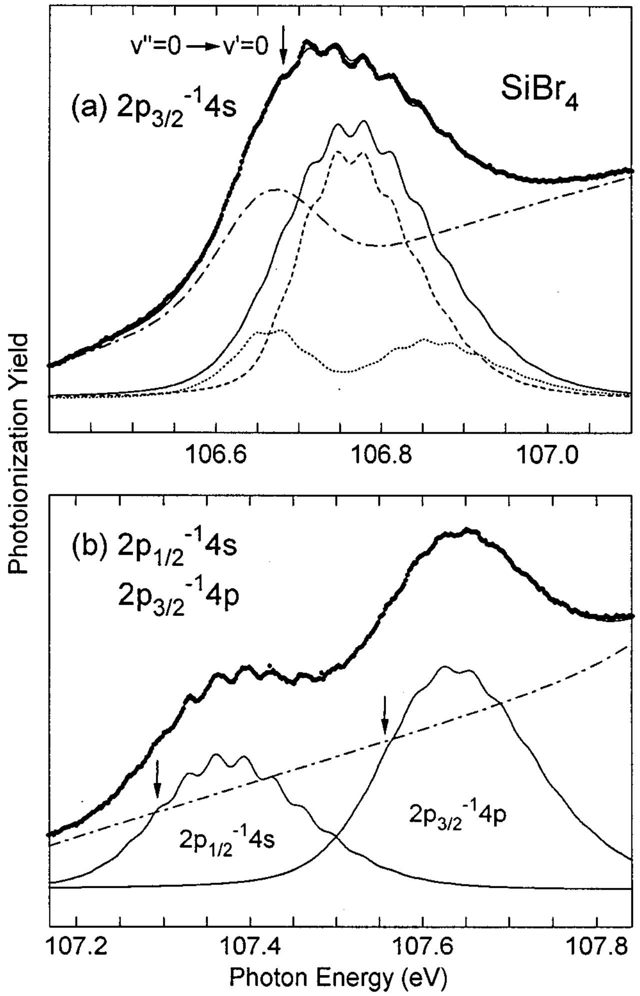

FIG. 4. Results of Franck-Condon analysis of the vibrationally split (a) Si-$2p_{3/2}^{-1}4s$, (b) Si-$2p_{1/2}^{-1}4s$, and Si-$2p_{3/2}^{-1}4p$ core excitations in SiBr$_4$. Solid subspectrum: Franck-Condon fits; dotted subspectrum: hot-band contributions; dashed subspectrum: without hot-band contributions. The arrows indicate the $v''=0\rightarrow v'=0$ excitations of the Rydberg states. Dash-dotted curve: background including a $2p^{-1}$ val transition.

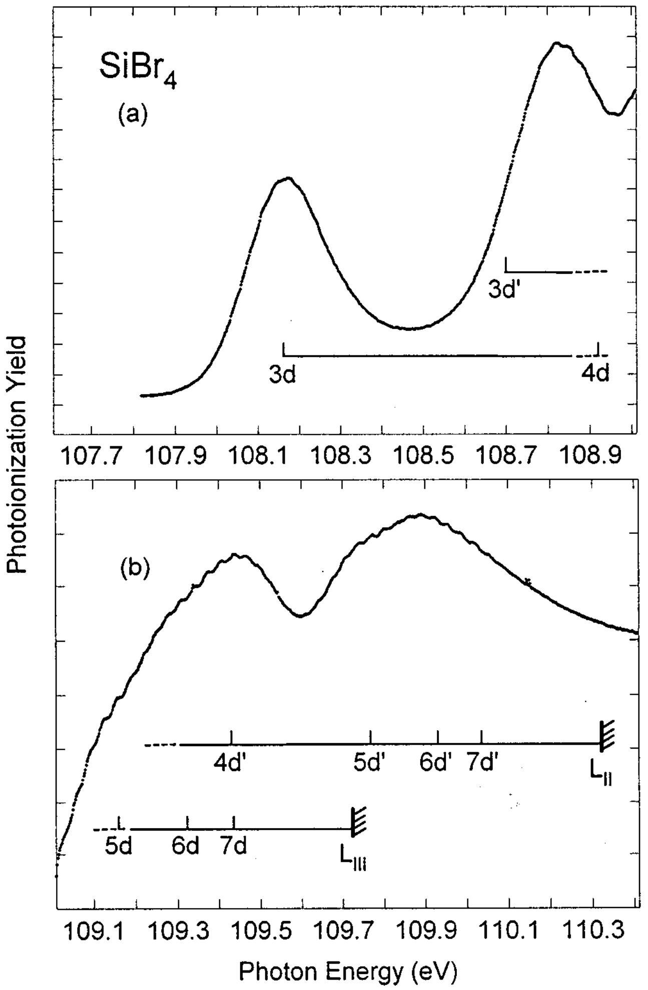

FIG. 5. Vibrationally split Si-$2p^{-1}nd$ excitation in SiBr$_4$: (a) Rydberg region with $2p_{3/2}^{-1}3d$, $4d(3d,4d)$, and $2p_{1/2}^{-1}3d$ $(3d')$; (b) Rydberg region with higher $2p^{-1}nd$ Rydberg states. The vertical bars mark the energies of the estimated $v''=0\rightarrow v'=0$ excitations of these Rydberg states (see text).

distances in the core-excited state of $R_e=2.103\pm0.002$ Å. The fits reveal two special properties [see Fig. 4(a)]: (i) Remarkably strong spectral features from ''hot bands'' are identified (dotted subspectrum), which represent excitations from ground-state vibrational states $v''=1,2,...$ to excited vibrational states of the electronically excited state ($v'=0,1,2,...$); they are so intense due to the low ground-state vibrational energy. The ''hot-band'' intensity is larger than for other molecules (e.g., SiCl$_4$, see below). In the dashed subspectrum, the ''non-hot-band'' contribution is given, i.e., from the usual $v''=0\rightarrow v'=0,1,2,...$ excitations. (ii) At $h\nu=106.65$ eV, a $2p_{1/2}^{-1}$ val feature is observed (dash-dotted subspectrum), which overlaps with the $2p_{3/2}^{-1}$ $4s$ Rydberg transition; for details, see Sec. IV. Similar vibrational energies as in the spectra of Fig. 4 are also observed in the $2p_{3/2}^{-1}3d$ and $2p_{1/2}^{-1}3d$ as well as $2p_{3/2}^{-1}4d,5d,6d,...$ and $2p_{1/2}^{-1}4d,5d,6d,...$ spectral features shown in Figs. 5(a) and 5(b), respectively. We also assume that an $e-t_2$ splitting of the Si-$2p^{-1}3d$ excitation and broad overlapping shape resonance structures at $h\nu=109.5-110.5$ eV occur, similarly to Si-$2p$ Rydberg excitation in SiCl$_4$ [16,10,30]; these effects hinder an adequate Franck-Condon analysis for the high-energy vibrational structures.

C. Silicon (IV) chloride, SiCl$_4$

As seen in Fig. 1, the Si-$2p$ spectrum of SiCl$_4$ is quite similar to that of SiBr$_4$, consisting also of excitations to a_1 and t_2 valence states as well as to Si-$2p^{-1}4s$, $4p$, and nd Rydberg states with a single vibrational splitting which is assigned to the symmetric-stretching a_1 mode. The $2p_{3/2}^{-1}4s$, $2p_{1/2}^{-1}4s$, and $2p_{3/2}^{-1}4p$ excitations are well separated, and the results of a Franck-Condon analysis of these spectral shapes are shown in Figs. 6(a) and 6(b). The following results are obtained: The vibrational energy in the electronic ground state, $\hbar\omega_1''=52.69$ meV [28], increases to $\hbar\omega_1'=58.1\pm0.5$ meV in the core-excited state; the anharmonicity in the core-excited state is $(x_1\hbar\omega_1)'=0.12\pm0.05$ meV, and the equilibrium distance decreases from $R_g=2.019$ Å [31] in the ground state to $R_e=1.953\pm0.003$ Å in the core-excited

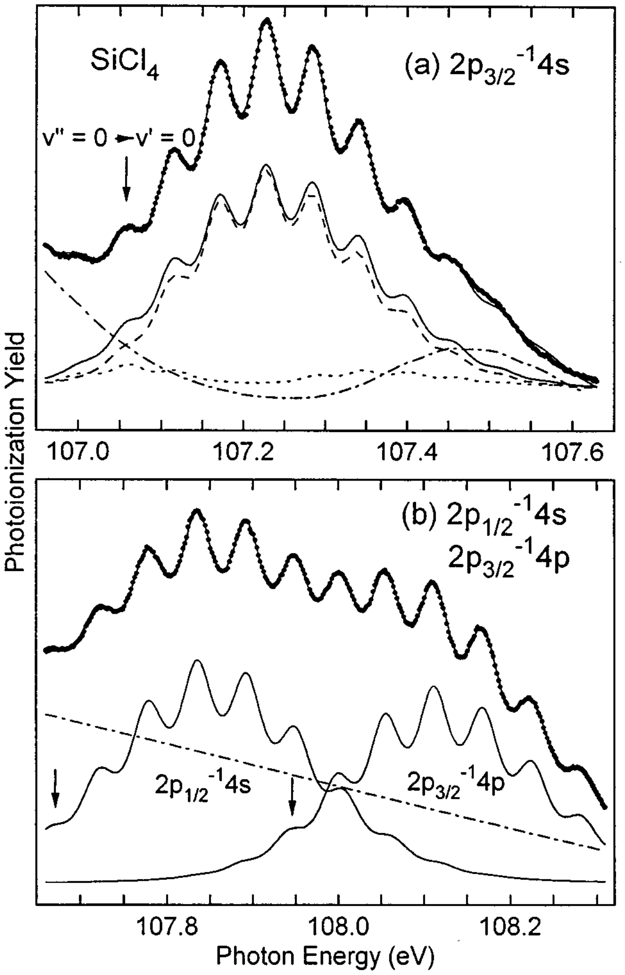

FIG. 6. Results of Franck-Condon analysis of (a) the Si-$2p_{3/2}^{-1}4s$ and (b) the Si-$2p_{1/2}^{-1}4s$, and Si-$2p_{3/2}^{-1}4p$ excitations in $SiCl_4$. The nomenclature is the same as in Fig. 4.

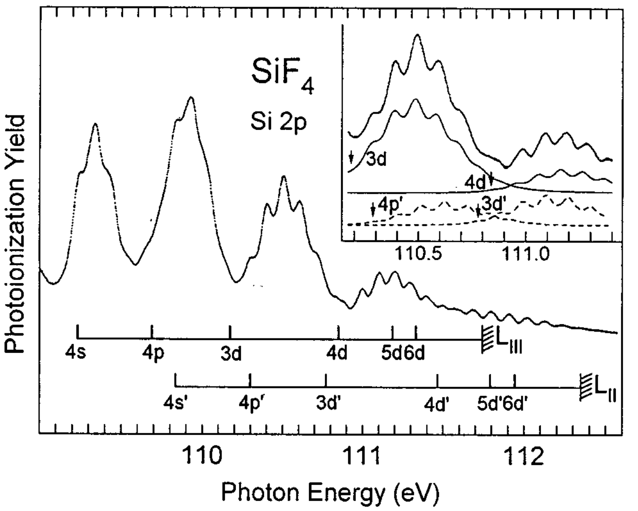

FIG. 7. Rydberg region of the Si-$2p$ photoabsorption spectrum of SiF_4. The observed resonances $2p_{3/2}^{-1}nl$ ($2p_{1/2}^{-1}nl$) are marked by nl (nl'); the vertical bar diagrams mark the $v''=0 \rightarrow v'=0$ excitations. Inset: Details of the spectral region dominated by the $2p^{-1}3d$ and $2p^{-1}4d$ excitations, with the subspectra resulting from the Franck-Condon analysis; the $v''=0 \rightarrow v'=0$ transitions are marked by vertical arrows. The solid (dashed) subspectra represent excitations from the Si-$2p_{3/2}$ (Si-$2p_{1/2}$) core state.

state. Again, spectral features from hot bands can be clearly identified (dotted subspectrum), even though they are weaker than in the spectrum of $SiBr_4$, due to the larger vibrational energy in $SiCl_4$. The spectrum in Fig. 6(a) also contains Si-$2p_{1/2}^{-1}t_2$ valence features in the energy region from 107.4 to 107.6 eV (dash-dotted subspectrum), which are identified by core-to-valence excitations that are not vanishing in *solid* $SiCl_4$ [10] (see also Sec. IV). More details on vibrational excitations and equilibrium distances are presented in Table II and in Ref. [16].

TABLE II. Summary of the results of the Franck-Condon analysis of the Rydberg regions of the Si-$2p$ core-excitation spectra of SiX_4 molecules: Vibrational energies $\hbar\omega''$ and $\hbar\omega'$, and intramolecular equilibrium distances R_g and R_e, in the ground and excited states, respectively. The force constant $\mathcal{F}$ for the Si-X symmetric-stretching modes, calculated on the basis of the vibrational ground-state energies, are also given. For comparison, the vibrational energies and equilibrium distances of the ionized $(Z+1)$ molecules, $PX_4{}^{+}$, are given in the last two columns. The numbers in parentheses represent the error bars in units of the last digit.

	$\hbar\omega''$ (meV)	$\mathcal{F}$ (m dyn) Å	$\hbar\omega'^{a}$ (meV)	R_g (Å)	$R_e{}^{a}$ (Å)	$-\Delta R^{a}$ (Å)	$\hbar\omega(PX_4{}^{+})$ (meV)	$R(PX_4{}^{+})$ (meV)
SiH_4	271.13[b]	2.81	298.5(1.0)	1.471[c]	1.416(1)	0.055(1)	284.5[d]	1.42(2)[e]
SiD_4	193.8[b]	2.87	212.9(1.0)	1.471[c]	1.416(1)	0.055(1)	205.1[d]	1.42(2)[e]
SiF_4	99.18[f]	7.16	109.0(2.0)	1.554[g]	1.486(2)	0.068(2)		
$Si(CH_3)_4$	73.47[h]	3.10	76.0(2.0)	1.888[h]	1.823(2)	0.065(2)		
$SiCl_4$	52.69[i]	3.72	58.1(0.5)	2.019[j]	1.953(3)	0.066(3)	55.8[k]	1.97(1)[l]
$SiBr_4$	30.87[i]	2.92	33.6(0.5)	2.150[m]	2.103(2)	0.047(2)	28.1[k]	

[a] This work.
[b] Reference [36].
[c] Reference [37].
[d] Reference [49].
[e] Reference [50].
[f] Reference [32].
[g] Reference [33].
[h] Reference [26].
[i] Reference [28].
[j] Reference [31].
[k] Reference [51].
[l] Reference [52].
[m] Reference [29].

D. Silicon (IV) fluorine, SiF_4

Figure 1 also gives an overview of the Si-2p core-excitation spectrum of SiF_4 with a_1 valence features that are farther away from the t_2 features than in the case of $SiBr_4$ and $SiCl_4$. In addition, the 4s transition is more intense in SiF_4 than in $SiCl_4$ and $SiBr_4$. In Fig. 7, the higher Rydberg region $2p^{-1}nd$ is shown, also revealing a single symmetric stretching vibration, which was fitted by a Franck-Condon analysis. The following Franck-Condon parameters were derived: The vibrational energy in the electronic ground state, $\hbar\omega_1'' = 99.18$ meV [32], increases to $\hbar\omega_1' = 109.0 \pm 2.0$ meV in the core-excited states, with anharmonicity in the core-excited state of $(x_1\hbar\omega_1)' = 0.45 \pm 0.15$ meV; the equilibrium distance decreases from $R_g = 1.554$ Å [33] in the electronic ground state to $R_e = 1.486 \pm 0.002$ Å in the core-excited state. In the case of the $2p^{-1}4s$ states, both stretching and bending vibrational modes are excited. This is caused by the mixed-valence–Rydberg character of this state, resulting in deviations from the T_d symmetry in the excited state. For more details, see Ref. [15] and Sec. V.

E. Silane: SiH_4 and SiD_4

For silane, both SiH_4 and SiD_4 were studied. This allows an easy separation of Rydberg states and vibrational substates, since the latter are strongly changed by an isotope effect on the vibrational energies, which diminishes vibrational energies by $\cong\sqrt{2}$ upon deuteration. In Fig. 8, the low-lying Rydberg transitions $2p_{3/2}^{-1}5s$, $2p_{1/2}^{-1}5s$, and $2p_{3/2}^{-1}3d(e/t_2)$ are shown with their intense vibrational sidebands; the given assignment of the vibrational states is based on the ground-state vibrational energies. The energy separation of vibrational substates from the $v''=0 \rightarrow v'=0$ Rydberg excitations are smaller by $\cong\sqrt{2}$ in SiD_4 as compared to SiH_4, both in case of the dashed substates (bending vibrations) and the solid substates (symmetric stretching vibrations). In addition, the $v''=0 \rightarrow v'=0$ excitations of all Rydberg states are shifted in SiD_4 by 25 meV to lower energies relative to SiH_4 [34]; this shift is caused by different zero-point vibrational energies in the electronic ground and excited states of SiH_4 and SiD_4 [34]. A close look at the vibrational substates reveals a *single* vibrational mode (i.e., the symmetric stretching mode) for the 3d excitations, but three vibrational modes of both stretching and bending character for the 5s excitations (see Fig. 8). The existence of a *single* vibrational mode continues to high ns and nd excitations (not shown here). Similar to SiF_4, the excitation of a bending vibrational mode reveals the mixed valence–Rydberg character of the $2p^{-1}5s$ state in silane, but with better separation and higher intensity of the bending vibrational modes.

The existence of bending modes reflects a change in the T_d symmetry of the ground state of silane toward a C_{2v} symmetry in core-excited silane. In SiH_4 (SiD_4), a Franck-Condon analysis is possible [35], resulting in $\hbar\omega_1'' = 271.13$ meV (193.8 meV) [36] $\rightarrow \hbar\omega_1' = 298.5 \pm 1.0$ meV (212.9 ± 1.0 meV), $\hbar\omega_2'' = 120.38$ meV (84.95 meV) [36] $\rightarrow \hbar\omega_2' = 131.1 \pm 1.0$ meV (92.6 ± 1.0 meV), $\hbar\omega_4'' = 113.25$ meV (83.6 meV) [36] $\rightarrow \hbar\omega_4' = 106.6 \pm 1.0$ meV (78.0 ± 1.0 meV). The Si-H equilibrium distances are approximately independent of H and D, with $R_g = 1.471$ Å [37] $\rightarrow R_a = 1.416 \pm 0.001$ Å, note that R_g (R_a) is the ground-state (averaged excited-state) equilibrium distance. By separating the four H atoms to H_1, H_2, H_3, and H_4, we obtain distortions in the distances by +0.006 and −0.006 Å for the Si-$H_{1;2}$ and Si-$H_{3;4}$ distances, respectively. The H-Si-H angles change from 109.5° to 122.5°±1.0°, to 102.5°±1.0°, and to 108.0°±0.5° for H_1-Si-H_2, H_3-Si-H_4, and H_i-Si-H_j (ij = 13,14,23,24), respectively; that is, we obtain a H_1-Si-H_2 spreading of 13° and a H_3-Si-H_4 narrowing of 7° as well as corresponding changes of the other angles. These distortions enable the nonsymmetric vibrational excitations. Further details were given in Ref. [35].

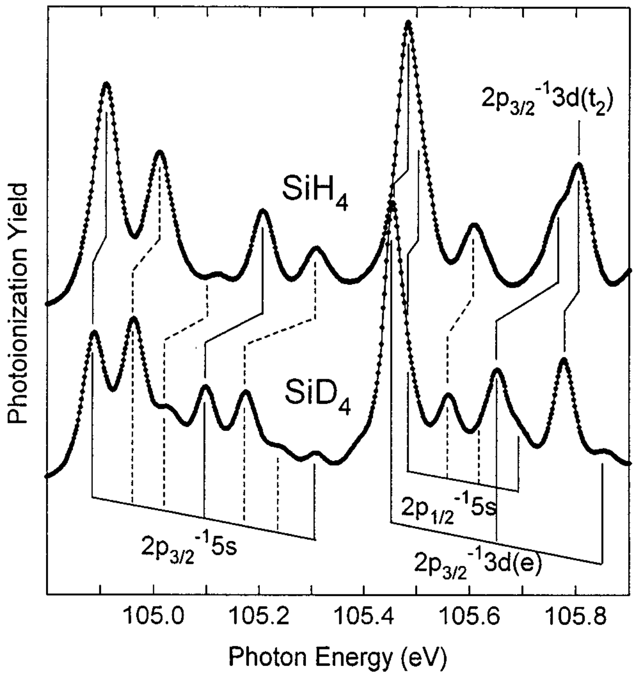

FIG. 8. Spectral regions of the lowest Rydberg excitations in the core-excitation spectra of SiH_4 (upper) and SiD_4 (lower), including the $2p_{3/2}^{-1}5s$, $2p_{1/2}^{-1}5s$, $2p_{3/2}^{-1}3d(e)$, and $2p_{3/2}^{-1}3d(t_2)$ resonances. Note that the energies of the $v''=0 \rightarrow v'=0$ excitations of SiH_4 and SiD_4 differ by 25 meV due to an isotopic effect on the zero-point vibrational energies (see Ref. [34]). The $v''=0 \rightarrow v'=0$ transitions and the excitations to symmetric-stretching-mode vibrational states are marked by solid vertical bars. Bending-mode vibrational states are identified by dashed vertical bars; these latter vibrations are clearly absent in case of the $2p_{3/2}^{-1}3d$ resonances.

IV. VALENCE STATES IN SiX_4 MOLECULES

A. Vibrationally split valence features

In the molecules studied, vibrational splitting of core-excited states can only be resolved well for Si-$2p^{-1}$ Ryd excitations. Nevertheless, in some cases vibrational substates have also been resolved for core-to-valence excitations: In Fig. 9, e.g., part of the Si-$2p^{-1}4a_1$ and Si-$2p^{-1}9t_2$ states are displayed for SiH_4/SiD_4 and SiF_4, respectively, showing well-resolved fine-structure features, i.e., vibrational substates. The vibrational energies of these substates are 83, 57, and 50 meV for SiH_4, SiD_4, and SiF_4, respectively. As expected, the vibrational energy for SiD_4 is smaller by a factor of $\sqrt{2}$ then that of SiH_4.

In all cases, the measured vibrational energies of the valence features are much smaller than in the case of the symmetric-stretching vibrational modes for high-*n* Rydberg states: *Bending* vibrational modes are obviously excited, similar to the well-resolved Si-$2p^{-1}5s$ vibrational substates in SiH_4 and SiD_4, and to the Si-$2p^{-1}4s$ in SiF_4, and this is due to molecular distortions, destroying T_d symmetry. To explain such distortions, two different mechanisms are known: (i) the first-order or normal Jahn-Teller effect, which requires degenerate states; and (ii) the second-order or pseudo Jahn-Teller effect, which applies to nondegenerate states.

In all SiX_4 molecules, the total electronic wave function of the electronic ground state has A_1 symmetry, and only final states with a T_2 symmetry in the total electronic wavefunction can be excited. This shows that in principle all excited states in SiX_4 molecules can undergo a first-order Jahn-Teller distortion. In Ref. [35], we show for silane that the triply degenerate Si-$2p$ core hole (t_2 symmetry) does not undergo a first-order Jahn-Teller distortion. The question whether the *excited* electron is in a degenerate or in a nondegenerate orbital results in a possible occurrence of a first-order Jahn-Teller distortion.

In case of SiH_4/SiD_4, the excited electron is in the $4a_1$ orbital; a first-order Jahn-Teller distortion is not possible. Consequently, we explain the observed bending modes by a second-order Jahn-Teller effect on the basis of calculations for the $(Z+1)$ molecule PH_4 [38]. In case of the Si-$2p^{-1}9t_2$ excitation in SiF_4, the situation is different. By neglecting the core hole, we do not have the excited electron in an a_1 orbital, but in a degenerate t_2 molecular orbital. In this case, a first-order Jahn-Teller effect is possible, which might also explain the observed bending vibrational modes.

The second-order Jahn-Teller effect can also be understood in a much more qualitative way following the valence-shell electron-pair repulsion theory (VSEPR) of Gillespie [39]. For the Si-$2p^{-1}$ val excitations of SiX_4 molecules, geometries close to the *ground*-state PX_4 [36] are expected, which is a radical with an unpaired electron. This unpaired electron interacts with the eight bonding electrons, and may lead to a molecular distortion as proven by calculations for PH_4 [38,40–42] and PF_4 [38]. These calculations result in one X-P-X angle that is distinctly larger than the 109.5° T_d angle (PH_4: 172° [38]; PF_4: 162° [38]); all other angles are slightly smaller than the tetrahedral angle of 109.47°. This distortion enables the excitation of bending-vibrational modes.

B. Valence-orbital region in $SiCl_4$ and $SiBr_4$

Figure 10 displays the valence region of $SiCl_4$ and $SiBr_4$. In both molecules, the lowest valence states are assigned to spin-orbit-coupled a_1 states, and a large variety of t_2 valence states is observed. The latter are indicated by arrows and exhibit at least seven (eight) states for $SiCl_4$ ($SiBr_4$). Note that valence states extending to the $4s$ region are essential to achieve reasonable fits in the Si-$2p^{-1}$ Ryd states. For $SiCl_4$, this valence state is also visible in the spectrum of solid $SiCl_4$ [10,43], whereas Rydberg states are quenched in the condensed phase. For $SiBr_4$, condensed-phase spectra are not available.

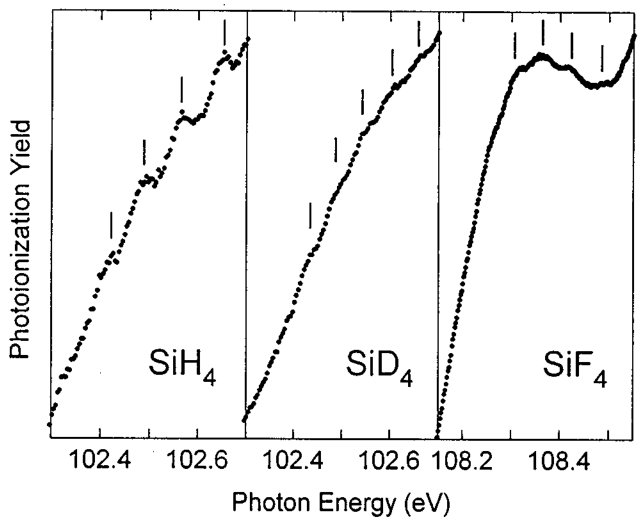

FIG. 9. Details of the Si-$2p_{3/2}^{-1}4a_1$ valence excitations in SiH_4 and SiD_4, as well as of the Si-$2p_{3/2}^{-1}9t_2$ state in SiF_4, with vibrational bending modes.

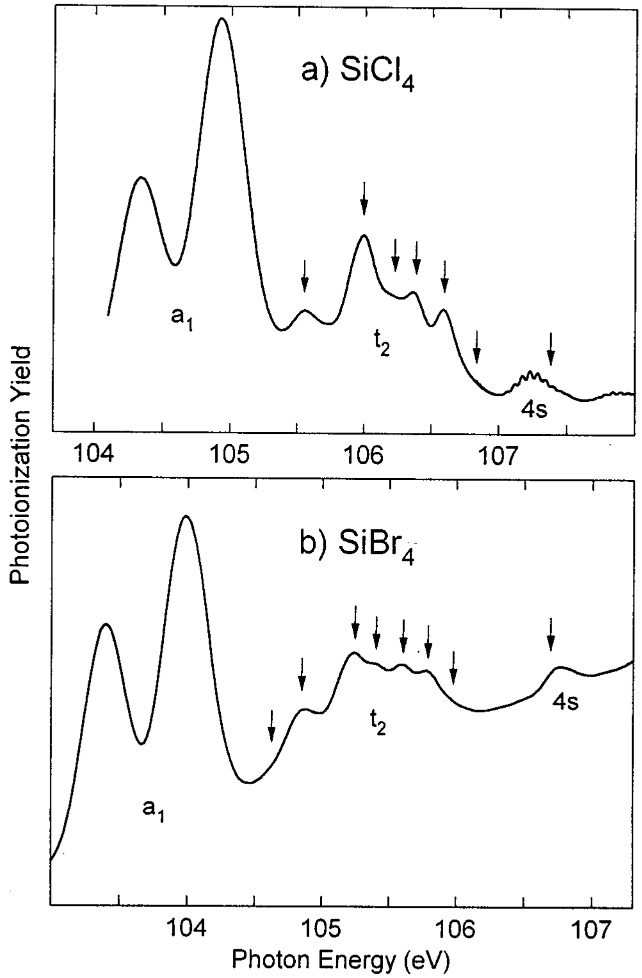

FIG. 10. Low-energy part of the Si-$2p^{-1}$ excitation spectra of (a) $SiCl_4$ and (b) $SiBr_4$, with the a_1 and t_2 valence states and the lowest Rydberg state $2p_{3/2}^{-1}4s$. All peaks assigned to the $2p^{-1}t_2$ multiplet are indicated with vertical arrows.

Ishikawa *et al.* [30] and Tse *et al.* [11] predicted only two valence orbitals with orbital orders a_1 and t_2 for $SiCl_4$, while for $SiBr_4$ no calculations exist. On the basis of these calculations, the large variety of peaks has to be assigned to $2p^{-1}t_2$ valence states both for $SiCl_4$ and $SiBr_4$. By considering only the triply degenerate t_2 valence orbital, with a possible first-order Jahn-Teller distortion, as well as the spin-orbit coupling of the core hole, we achieve six different states at most. This number is obviously too small for the observed structures. However, we may consider an interaction between the core hole and the excited electron, which would lead to an increase of the number of final states. This has been shown in Ref. [44] for the S $2p^{-1}3b_1$ valence state in SO_2 with five electronic substates, increasing the three possible electronic substates by using only spin-orbit splitting and ligand-field splitting of the core hole. Only an additional consideration taking the core-hole excited-orbital interaction into account, can explain the complete spectral structure.

V. COMPARISON OF $2p^{-1}$ Ryd CORE-EXCITATION SPECTRA OF TETRAHEDRAL SiX_4 MOLECULES

A. Franck-Condon analyses

In Table II, the results of the Franck-Condon analysis of the symmetric stretching vibrational modes in the Rydberg region are summarized, i.e., the vibrational energy $\hbar\omega'$ and the equilibrium distance R_e in the excited state obtained from the vibrational energy $\hbar\omega''$ and the equilibrium distance R_g in the ground state. Also given is $\Delta R = R_e - R_g$ for the SiX_4 (X=H, D, F, CH_3, Cl, Br) molecules. In addition, frequencies and equilibrium distances for the $(Z+1)$ molecule, P${X_4}^+$, taken from the literature, are listed, which is equivalent to highly excited SiX_4 Rydberg states. The vibrational energies and equilibrium distances of the core-excited molecules are in close agreement with the values listed in the last two columns of Table II for the valence-ionized $(Z+1)$ molecules P${X_4}^+$, supporting the concept of the equivalent-cores approximation.

For comparism, the force constants $\mathcal{F}$ for the Si-X symmetric-stretching vibrational mode of the ground-state molecules [$\mathcal{F}=(\hbar\omega'')^2\times m^*$] are also given (where m^* is the reduced mass). In most cases, both $\hbar\omega'$ and $\hbar\omega''$ decreases with $\sqrt{m^*}$, i.e., the force constant is nearly constant. This is approximately valid for most of the SiX_4 molecules, with the exception of SiF_4, and to a smaller extent also of $SiCl_4$. In particular, SiF_4 exhibits, both in the ground state and in the core-excited states, vibrational energies that are higher than expected: e.g., the SiF_4 vibrational energies are higher than those of $Si(CH_3)_4$, despite $m_{\mathrm{F}} \geqslant m_{\mathrm{CH}_3}$. This can be explained by a partial double-bond character of the Si-F, and in case of the $(Z+1)$ molecule, of the P-F bond [39]. This is due to a delocalization of the unshared electron pairs of florine which are nonbonding F-2p electrons, to the incomplete valence shell of the central atom, i.e., the unoccupied Si-3d or P-3d orbitals. This will lead to a subsequent increase of the vibrational energy as well as the force constant $\mathcal{F}$. In contrast to this, Cl and Br also have unoccupied d orbitals in their valence shell, and consequently the Cl-3p and Br-4p electrons do not delocalize to the central atom.

TABLE III. Experimental and theoretical [45] linewidths of Si-$2p^{-1}$ excitations in SiX_4 molecules.

	Experiment (meV)	Theory [45] (meV)
SiH_4	50(5)	32
SiD_4	50(5)	32
SiF_4	85(10)	14
$Si(CH_3)_4$	76(9)	37
$SiCl_4$	48(2)	32
$SiBr_4$	39(6)	

It is also observed that the core-excited states in all molecules have vibrational energies of the symmetric-stretching vibrational mode, which are about 8% larger than in the electronic ground state. This can be understood by a shrinking of the molecules by ≅0.06 Å upon excitation, caused by a steeper attractive part of the potential surface that originates from an electron configuration without a change of the repulsive part. As a consequence, the potential surface becomes narrower and the vibrational energy increases.

The spectra reveal that the lowest Rydberg states in SiH_4, SiD_4, and SiF_4 exhibit the symmetric-stretching vibrational mode *as well as* bending-vibrational modes. These bending-vibrational modes are due to a lowering of the symmetry, which is caused by a second-order Jahn-Teller effect [35]. In $SiCl_4$ and $SiBr_4$, these additional modes are clearly missing, and in $Si(CH_3)_4$, the lowest Rydberg states overlap strongly with the valence states, i.e., no statement on the excitation of bending-vibrational modes can be given in this case.

B. Natural lifetime width

Table III gives a summary of the fitted experimental and theoretical natural lifetime widths of the studied molecules. The theoretical values were calculated by McColl and Larkins [45] using a one-center model, which considers only the Auger channels that create two holes in the valence shell at the Si site, and neglect correlation effects of the electrons beyond the Hartree-Fock approximation. For all studied SiX_4 molecules, the experimental lifetime widths are larger than the theoretical values. In case of SiH_4, SiD_4, and $SiCl_4$, the experimental lifetime widths are ≅50% larger than the theoretical values; for $Si(CH_3)_4$, the experimental value is ≅100% larger; and in case of SiF_4, the experimental value is by a factor of 6 even larger than the theoretical value. Note that the experimental lifetime widths were obtained for core-excited states, but the theoretical values were calculated for core-ionized states. Larkins pointed out that the lifetime width of a core-excited state can be up to 20% larger than the lifetime width of an ionized state [46]; however, this can only explain a small part of the discrepancy between theory and experiment.

The largest difference between experiment and theory is found for SiF_4. In this case, the Auger spectrum shows some peculiarities that were explained in terms of electron correlation in Refs. [47] and [48]; the one-center model cannot reproduce all features in the spectrum [46]. The lifetime widths depend on the total Auger rates, i.e., the Auger channels, which can only be explained by correlation, also contribute to the observed lifetime width. We may therefore assume that correlation effects can influence the lifetime widths, explaining the differences between experiment and theory.

From the number of valence electrons and the size of the molecules, we obtain a decreasing valence-electron density and decreasing electron-correlation effects from F to Cl to Br. The correlation effect can explain the sequence $\Gamma_F > \Gamma_{Cl} > \Gamma_{Br}$. Nevertheless, more accurate calculations are necessary to clarify the contributions of electron-correlation effects to the natural lifetime widths.

VI. SUMMARY AND CONCLUSIONS

In summary, we resolved vibrational fine structures in the Si-$2p$ core-excitation spectra of SiX_4 molecules using high-resolution photoionization spectroscopy. A symmetric-stretching vibrational splitting could be resolved for all Rydberg states. For the lowest Rydberg states in SiH_4, SiD_4, and SiF_4, bending-mode vibrations were observed, which depend on the mixed-state character of these resonances. Franck-Condon analyses of the vibrationally resolved spectral shapes were performed, and the derived results for vibrational energies and intramolecular distances were found to be in good agreement with the $(Z+1)$ approximation. The experimental lifetime widths of the molecules are compared to calculated values, revealing a substantial discrepancy for SiF_4.

In the core-to-valence excitation region of silane and SiF_4, the excitation of a bending-vibrational mode was identified, caused by Jahn-Teller effects. The rich fine structure of the Si-$2p^{-1}t_2$ excitations of $SiCl_4$ and $SiBr_4$ is assigned to an interaction between the excited electron and the created core hole.

ACKNOWLEDGMENTS

This work was supported by the Bundesminister für Bildung, Wissenschaft, Forschung und Technologie, Project No. 05-650-KEA, and the Deutsche Forschungsgemeinschaft, Project No. DO 561/1-1.

[1] S. Bodeur, I. Nenner, and P. Millie, Phys. Rev. A **34**, 2986 (1986).
[2] D. G. J. Sutherland, G. M. Bancroft, J. D. Bozek, and K. H. Tan, Chem. Phys. Lett. **199**, 341 (1992).
[3] W. Hayes, F. C. Brown, and A. B. Kunz, Phys. Rev. Lett. **27**, 774 (1971).
[4] W. Hayes and F. C. Brown, Phys. Rev. A **6**, 21 (1972).
[5] M. B. Robin, Chem. Phys. Lett. **31**, 140 (1975).
[6] H. Friedrich, B. Pittel, P. Rabe, W. H. E. Schwarz, and B. Sonntag, J. Phys. B **13**, 25 (1980).
[7] J. D. Bozek, G. M. Bancroft, and K. H. Tan, Chem. Phys. **145**, 131 (1990).
[8] T. M. Zimkina and A. S. Vinogradov, J. Phys. Colloq. **32**, C4-3 (1971).
[9] J. D. Bozek, K. H. Tan, G. M. Bancroft, and T. S. Tse, Chem. Phys. Lett. **138**, 33 (1987).
[10] R. A. Rosenberg and S. P. Frigo, Chem. Phys. Lett. **184**, 439 (1991).
[11] J. S. Tse, Z. F. Liu, J. D. Bozek, and G. M. Bancroft, Phys. Rev. A **39**, 1791 (1989).
[12] R. A. Rosenberg, C.-R. Wen, K. Tan, and J.-M. Chen, J. Chem. Phys. **92**, 5196 (1990).
[13] J. D. Bozek, G. M. Bancroft, J. N. Cutler, and K. H. Tan, Phys. Rev. Lett. **65**, 2757 (1990).
[14] J. D. Bozek, G. M. Bancroft, and K. H. Tan, Phys. Rev. A **43**, 3597 (1991).
[15] R. Püttner, M. Domke, K. Schulz, and G. Kaindl, Chem. Phys. Lett. **250**, 145 (1996).
[16] M. Domke, R. Püttner, K. Schulz, and G. Kaindl, Phys. Rev. A **52**, 1147 (1995).
[17] R. Püttner, M. Domke, and G. Kaindl, Acta Phys. Pol. **91**, 865 (1997).
[18] M. Domke, T. Mandel, A. Puschmann, C. Xue, D. A. Shirley, G. Kaindl, H. Petersen, and P. Kuske, Rev. Sci. Instrum. **63**, 80 (1992).
[19] R. N. S. Sodhi and C. Brion, J. Electron Spectrosc. Relat. Phenom. **34**, 363 (1984).
[20] E. Hutchisson, Phys. Rev. **36**, 410 (1930).
[21] E. Hutchisson, Phys. Rev. **37**, 45 (1931).
[22] H. Nakamatsu, Chem. Phys. **200**, 49 (1995).
[23] J. L. Dehmer, A. C. Parr, and S. H. Southworth, in *Handbook of Synchrotron Radiation*, Vol. 2, edited by G. V. Marr (Elsevier, Amsterdam, 1987).
[24] H. Friedrich, B. Sonntag, P. Rabe, W. Butcher, and W. H. E. Schwarz, Chem. Phys. Lett. **64**, 360 (1979).
[25] R. N. S. Sodhi, S. Daviel, and C. E. Brion, J. Electron Spectrosc. Relat. Phenom. **35**, 45 (1985).
[26] L. M. Sverdlov, M. A. Kovner, and E. P. Krainov, *Vibrational Spectra of Polyatomic Molecules* (Wiley, New York, 1974) p. 560.
[27] K. Shimizu and H. Murata, J. Mol. Spectrosc. **5**, 44 (1960).
[28] *Tables of Molecular Vibrational Frequencies, Consolidated Vol. I*, edited by T. Shimanouchi, Natl. Bur. Stand. U.S. Ref. Data Ser. No. 39 (U.S. GPO, Washington, DC, 1972), p. 23.
[29] *Gmelins Handbuch der Anorganischen Chemie*, 8th ed., edited by A. Kotowski, G. Hantke, G. Kirschstein, F. Seuferling, and K. Swars, Phosphorus Vol. 16C (Verlag Chemie, Weinheim, 1965), p. 376.
[30] H. Ishikawa, K. Fujima, H. Adachi, E. Miyauchi, and T. Fujii, J. Chem. Phys. **94**, 6740 (1991).
[31] R. R. Ryan and K. Hedberg, J. Chem. Phys. **50**, 4986 (1969).
[32] *Gmelin Handbook of Inorganic Chemistry*, 8th ed., edited by G. Hönes, H. Keller-Rudek, D. Koschel, P. Merlet, H. Schäfer, and F. Schröder, Silicon Supplement Vol. B7 (Springer, Berlin, 1992), p. 156.
[33] *Structure Data of Free Polyatomic Molecules*, edited by K.-H. Hellwege and A. M. Hellwege, Landolf-Börnstein, New Series, Group II, Vol. 15 (Springer, Berlin, 1987), p. 96.
[34] R. Püttner, M. Domke, D. Lentz, and G. Kaindl, J. Phys. B **29**, L565 (1996).

[35] R. Püttner, M. Domke, D. Lentz, and G. Kaindl, Phys. Rev. A **56**, 1228 (1997).

[36] *Gmelin Handbook of Inorganic Chemistry*, 8th ed., edited by H. Keller-Rudek, D. Koschel, U. Krüerke, and P. Merlet, Silicon Supplement, Vol. B1 (Springer, Berlin, 1982), p. 94.

[37] *Structure Data of Free Polyatomic Molecules*, edited by K. Kuchitsu, Landolt-Börnstein, New Series, Group II, Vol. 21 (Springer, Berlin, 1992), p. 96.

[38] J. M. Howell and J. F. Olsen, J. Am. Chem. Soc. **98**, 7119 (1976).

[39] R. J. Gillespie, J. Chem. Educ. **40**, 295 (1963).

[40] D. Gonbeau, M.-F. Guimon, J. Ollivier, and G. Pfister-Guillouzo, J. Am. Chem. Soc. **108**, 4760 (1986).

[41] A. Demolliens, O. Eisenstein, P. C. Hilberty, J. M. Lefour, G. Ohanessian, S. S. Shaik, and F. Volatron, J. Am. Chem. Soc. **111**, 5623 (1989).

[42] C. J. Cramer, J. Am. Chem. Soc. **113**, 2439 (1991).

[43] J.-M. Chen, R. Klauser, S.-C. Yang, and C.-R. Wen, Chem. Phys. Lett. **246**, 285 (1995).

[44] N. A. Shklyaeva, L. N. Mazalov, and V. V. Murakhtanov, J. Struct. Chem. **20**, 621 (1979).

[45] J. McColl and F. P. Larkins, Chem. Phys. Lett. **196**, 343 (1992).

[46] F. P. Larkins, Aust. J. Phys. **49**, 457 (1996).

[47] F. P. Larkins, J. McColl, and E. Z. Chelkowska, J. Electron Spectrosc. Relat. Phenom. **67**, 275 (1994).

[48] F. Tarantelli and L. S. Cederbaum, Phys. Rev. Lett. **71**, 649 (1993).

[49] J. R. Durig, D. J. Antion, and F. G. Baglin, J. Chem. Phys. **49**, 666 (1968).

[50] *Gmelin Handbook of Inorganic Chemistry*, 8th ed., edited by W. Behrendt, U. W. Gerwarth, R. Hauboldt, J. v. Jouanne, H. Keller-Radek, D. Koschel, H. Schäfer, and J. Wagner, Phosphorus Supplement Vol. C1 (Springer, Berlin, 1993), p. 315.

[51] *Gmelins Handbuch der Anorganischen Chemie*, 8th ed., edited by A. Kotowski, Silicon Vol. 15B (Verlag Chemie, Weinheim, 1959), p. 317.

[52] W. F. Zelezny and N. C. Baenziger, J. Am. Chem. Soc. **74**, 6151 (1952).